

SANDIA REPORT

SAND2012-2323

Unlimited Release

Printed March 2012

Fundamental hydrogen interactions with beryllium: a magnetic fusion perspective

Robert D. Kolasinski, Norman C. Bartelt, Josh A. Whaley, Thomas E. Felter, and William R. Wampler

Prepared by
Sandia National Laboratories
Albuquerque, New Mexico 87185 and Livermore, California 94550

Sandia is a multiprogram laboratory operated by Sandia Corporation, a Lockheed Martin Company, for the United States Department of Energy's National Nuclear Security Administration under Contract DE-AC04-94AL85000.

Approved for public release; further dissemination unlimited.

Issued by Sandia National Laboratories, operated for the United States Department of Energy by Sandia Corporation.

NOTICE: This report was prepared as an account of work sponsored by an agency of the United States Government. Neither the United States Government, nor any agency thereof, nor any of their employees, nor any of their contractors, subcontractors, or their employees, make any warranty, express or implied, or assume any legal liability or responsibility for the accuracy, completeness, or usefulness of any information, apparatus, product, or process disclosed, or represent that its use would not infringe privately owned rights. Reference herein to any specific commercial product, process, or service by trade name, trademark, manufacturer, or otherwise, does not necessarily constitute or imply its endorsement, recommendation, or favoring by the United States Government, any agency thereof, or any of their contractors or subcontractors. The views and opinions expressed herein do not necessarily state or reflect those of the United States Government, any agency thereof, or any of their contractors.

Printed in the United States of America. This report has been reproduced directly from the best available copy.

Available to DOE and DOE contractors from

U.S. Department of Energy
Office of Scientific and Technical Information
P.O. Box 62
Oak Ridge, TN 37831

Telephone: (865) 576-8401
Facsimile: (865) 576-5728
E-Mail: reports@adonis.osti.gov
Online ordering: <http://www.osti.gov/bridge>

Available to the public from

U.S. Department of Commerce
National Technical Information Service
5285 Port Royal Rd.
Springfield, VA 22161

Telephone: (800) 553-6847
Facsimile: (703) 605-6900
E-Mail: orders@ntis.fedworld.gov
Online order: <http://www.ntis.gov/help/ordermethods.asp?loc=7-4-0#online>



SAND2012-2323
Unlimited Release
Printed March 2012

Fundamental hydrogen interactions with beryllium: a magnetic fusion perspective

Robert D. Kolasinski^(a), Norman C. Bartelt^(b), Josh A. Whaley^(a), Thomas E. Felter^(a), and William R. Wampler^(c)

^(a)Hydrogen and Metallurgical Science Department
Sandia National Laboratories
P.O. Box 969
Livermore, California 94550-MS9161

^(b)Materials Physics Department
Sandia National Laboratories
P.O. Box 969
Livermore, California 94550-MS9161

^(c)Radiation-Solid Interaction Department
Sandia National Laboratories
P.O. Box 5800
Albuquerque, New Mexico 87185-MS1056

Abstract

Increasingly, basic models such as density functional theory and molecular dynamics are being used to simulate different aspects of hydrogen recycling from plasma facing materials [1,2]. These models provide valuable insight into hydrogen diffusion, trapping, and recombination from surfaces, but their validation relies on knowledge of the detailed behavior of hydrogen at an atomic scale. Despite being the first wall material for ITER, basic single crystal beryllium surfaces have been studied only sparsely from an experimental standpoint. In prior cases researchers used electron spectroscopy to examine surface reconstruction or adsorption kinetics during exposure to a hydrogen atmosphere [3]. While valuable, these approaches lack the ability to directly detect the positioning of hydrogen on the surface. Ion beam techniques, such as low energy ion scattering (LEIS) and direct recoil spectroscopy (DRS), are two of the only experimental approaches capable of providing this information.

In this study, we applied both LEIS and DRS to examine how hydrogen binds to the Be(0001) surface. Our measurements were performed using an angle-resolved ion energy spectrometer (ARIES) to probe the surface with low energy ions (500 eV - 3 keV He⁺ and Ne⁺).

We were able to obtain a “scattering maps” of the crystal surface [4], providing insight on how low energy ions are focused along open surface channels. Once we completed a characterization of the clean surface, we dosed the sample with atomic hydrogen using a heated tungsten capillary. A distinct signal associated with adsorbed hydrogen emerged that was consistent with hydrogen residing between atom rows. To aid in the interpretation of the experimental results, we developed a computational model to simulate ion scattering at grazing incidence [5]. For this purpose, we incorporated a simplified surface model into the Kalypso molecular dynamics code [6]. This approach allowed us to understand how the incident ions interacted with the surface hydrogen, providing confirmation of the preferred binding site.

[1] A. Allouche, Phys. Rev. B, **78** (2008) 085429.

[2] R. Stumpf and P.J. Feibelman, Phys. Rev. B, **51** (1995) 13784.

[3] K. Pohl and E.W. Plummer, Phys. Rev. B, **59** (1999) R5324.

[4] R.D. Kolasinski, J.A. Whaley, and R. Bastasz, Phys. Rev. B, **79** (2009) 075416.

[5] R.D. Kolasinski, N.C. Bartelt, J.A. Whaley, and T.E. Felter, Phys. Rev. B (in press.)

[6] M.A. Karolewski, Nucl. Instr. Meth. B, **230** (2005) 402.

ACKNOWLEDGMENTS

It is a pleasure to acknowledge Robert Bastasz, Dean Buchenauer, and Rion Causey for helpful suggestions regarding this work. Sandia National Laboratories is a multi-program laboratory managed and operated by Sandia Corporation, a wholly owned subsidiary of Lockheed Martin Corporation, for the U.S. Department of Energy's National Nuclear Security Administration under contract DE-AC04-94AL85000.

Contents

1	Executive Summary	3
2	Introduction.....	5
2.1	Motivation.....	5
2.2	Low energy ion scattering and direct recoil spectroscopy	7
3	Experimental hardware.....	11
4	Analyzing polycrystalline beryllium surfaces.....	13
4.1	Characterizing adsorbed oxygen with Auger electron spectroscopy.....	15
5	Analyzing single crystal beryllium surfaces	17
5.1	Sample preparation	17
5.2	Hydrogen-dosed experiments	18
6	Developing a new theoretical framework for modeling scattering experiments	23
7	Time of flight system for impact collision ion scattering spectroscopy (ICISS)	25
7.1	Detecting backscattered particles: Impact collision ion scattering spectroscopy	25
7.2	Detecting forward scattered particles via time-of-flight	29
8	Summary of Results / Outlook	31
8.1	Future modeling pathway.....	31
	References.....	33

(This page intentionally left blank.)

1 Executive Summary

Additional details appear in: R. D. Kolasinski, N. C. Bartelt, J. A. Whaley, and T. E. Felter, *Phys. Rev. B* **85**, 115422 (2012).

The experimental fusion reactor ITER is designed to demonstrate the controlled ignition and extended burn of deuterium-tritium plasmas, representing a landmark achievement in magnetic fusion. Beryllium will be the principal plasma facing material in ITER and understanding how it interacts with hydrogen is crucial for modeling hydrogen recycling from the first wall. Uncertainties in key physical parameters associated with recombination, diffusion, and trapping have impeded efforts to develop detailed models of recycling.¹ While some progress has been made recently in resolving these issues for divertor-relevant materials (e.g. the W+H and C+H systems)² by using fundamental models of hydrogen in metals, there is virtually no comparable effort within the U.S. for the Be+H system – despite beryllium comprising over 80% of the interior surface of ITER. One of the main goals of this LDRD is to provide the understanding of the basic atomic-scale events that govern hydrogen recycling from beryllium surfaces.

In this study, we used low energy ion scattering (LEIS) and direct recoil spectroscopy (DRS) to probe single crystal beryllium surfaces in order to better understand the atomic-scale behavior of hydrogen. These two methods are unique in that they offer the capability to *directly* detect surface-adsorbed hydrogen and offer detailed information on its behavior. To perform the measurements, we used an angle-resolved ion energy spectrometer (ARIES) at Sandia/CA that was uniquely suited for such measurements, having been optimized to detect forward scattered and recoiled particles (the ideal geometry for examining light adsorbates.) Using this approach, we examined the Be(0001)+H(ads) system. We were able to obtain a “scattering maps” of the crystal surface, providing insight into how low energy ions are focused along open surface channels. Once we completed a characterization of the clean surface, we dosed the sample with atomic hydrogen. A distinct signal associated with adsorbed hydrogen emerged that was consistent with hydrogen residing between atom rows on the surface.

A key accomplishment of this LDRD has been the development of a variety of modeling tools to aid in the interpretation of scattering data. The theoretical framework needed to interpret such experiments is still rudimentary. By applying novel molecular dynamics techniques to the problem, we were able to make considerable advancements to how low energy scattering is modeled, especially at grazing incidence.

Finally, we developed a unique time of flight experimental detection capability for our ARIES instrument. As the name implies, this system involves measuring ion flight times (rather than using electrostatic methods) to determine ion energies. This type of detection system has two major advantages. First, it is sensitive to both ions and neutral particles, thereby removing a key uncertainty from modeling the experimental data. In addition, it reduces the dose required to obtain a measurement by a factor of 10^4 compared with more conventional detection techniques. Our preliminary measurements from this analysis indicate that this new approach will open up a wealth of new research projects that were not previously possible.

(This page intentionally left blank.)

2 Introduction

Once completed, the magnetic fusion reactor ITER will demonstrate for the first time controlled ignition and extended burn of deuterium-tritium plasmas. Because beryllium will be the principal plasma-facing material in the reactor, understanding how it interacts with hydrogen is particularly important. There has been a strong desire to understand hydrogen recycling, implantation, diffusion, and recombination from beryllium surfaces from a fundamental, atomic-scale perspective using first-principles modeling techniques. Examining how hydrogen binds and interacts with basic single crystal systems is an ideal way to validate model predictions. The Be(0001)+H system is particularly interesting because it is an example of a low-index, low-Z system which has been sparsely studied. While reconstructions of Be(0001) induced by H adsorption have been examined using electron diffraction and spectroscopy techniques,^{3,4} such methods do not provide direct sensitivity to the adsorbate configuration.

One of the few experimental techniques sensitive to adsorbed hydrogen is ion scattering. In this LDRD program, our plan was to apply this approach to understanding the atomic-scale details of hydrogen on beryllium surfaces. The motivation for this work and the basic concepts underlying ion scattering are discussed in the following sections.

2.1 Motivation

The interpretation of results from major confinement devices would benefit greatly from accurate models of hydrogen recycling from the surface. Recycling, the uptake and release of hydrogen from the first-wall, affects the plasma boundary layer and thus energy balance between the plasma and the external system.⁵ Of particular interest for the present discussion are “refined wall models,” which emphasize the details of the material response to plasma exposure.⁶⁻⁸ Recombination, particle impact desorption of hydrogen on surfaces, and diffusion of hydrogen into the material all contribute to recycling, as illustrated in Figure 1. As discussed in more detail in Refs. 6-8, each of these processes can be incorporated into a coupled set of differential equations with sets of phenomenological parameters. Given values for these parameters calculations of hydrogen uptake and release from plasma-facing materials are enabled. However, recycling from beryllium presents unique challenges because the detailed physics underlying many of the model inputs is not known – indeed many of these processes are very difficult to study experimentally. For example, the measured values of the recombination coefficient for beryllium are scattered over many orders of magnitude.⁹ A similar situation exists for the diffusion coefficients, where trends in the experimental data are obscured by uncertainties due to experimental effects (e.g. oxide accumulation on surfaces.)¹⁰ Desorption cross-sections and trapping are more amenable to accurate experimental observation, but a more detailed understanding of these processes for the Be+H system would certainly be welcome. The overall goal of the work described in this LDRD program is to provide understanding of the basic atomic-scale events that govern these microscale processes.

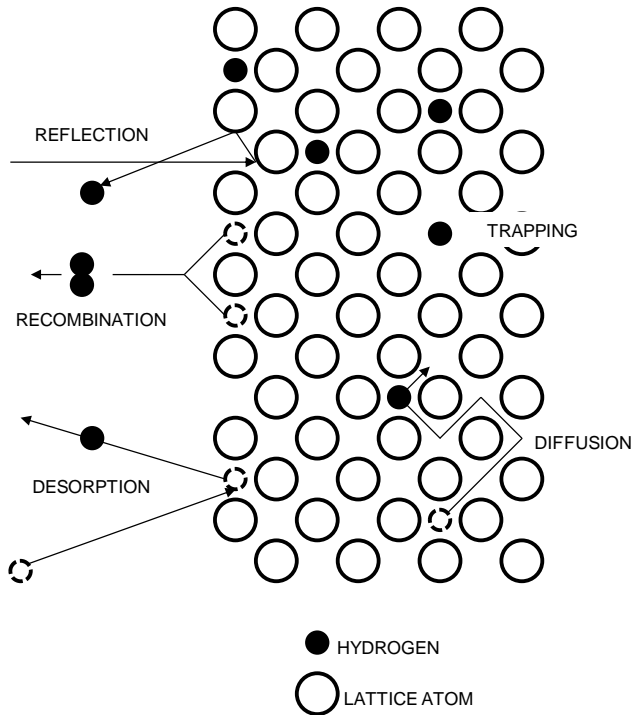


Figure 1: Schematic of processes that contribute to hydrogen recycling in beryllium.

How can fundamental modeling approaches (MD and DFT) be applied to addressing these problems? If the configuration of hydrogen on the surface is known, one can model the recombination by using energetic barriers computed using DFT, as was done by Vegge for the Mg(0001)+H system.¹¹ Similarly, DFT lends itself well to modeling diffusion and trapping energies, as has been demonstrated by Johnson and Carter.¹²

A necessary first step in developing and validating atomic models of recombination is knowledge of the binding geometry of H on Be. As eloquently described by Stumpf & Feibelman in 1995,¹³ the various experimental probes which have been applied to this problem have not yielded a self-consistent atomistic picture. On close-packed metal

surfaces, H often binds to a small number of well-defined binding sites [e.g. H/Ni(111)¹⁴], leaving the metal substrate structure intact. It is clear, however, that H/Be(0001) is not so simple. Based on DFT calculations, Stumpf & Feibelman proposed that depending on H coverage, Be reconstructs by forming networks of surface vacancies, as illustrated in Figure 2. Pohl & Plummer used LEED to show that the 1ML structure below room temperature is at least consistent with the existence of these vacancies. There is, however, still no clear picture of the temperature or coverage dependence of the adsorption. The theoretical challenge is revealed by Stumpf & Feibelman – there are numerous competing configurations of the surface which differ in energy by a few 10's of meV. (For instance the three configurations in Figure 2 only differ by 18meV/H.) These energies are within the uncertainty of DFT, making it unlikely that DFT can predict the precise ground state. Further, since these energy differences are much smaller than the wall thermal energies in fusion reactors, the surface will likely consist of a complex mix of such structures. Finally, since these reconstructions require the generation of Be vacancies, it is unclear whether the equilibrium states governed by adsorption energies can be reached.

As a pathway toward resolving these ambiguities, the objective of this work was to directly measure the binding geometry of hydrogen experimentally. For this purpose, we used low energy ion scattering and direct recoil spectroscopy, two ion beam techniques uniquely suited for measuring the configuration of hydrogen on surfaces. As detailed in the following sections, such measurements in principle provide exactly the needed information about the atomic-scale behavior of hydrogen on beryllium. They are, for example, sensitive to the

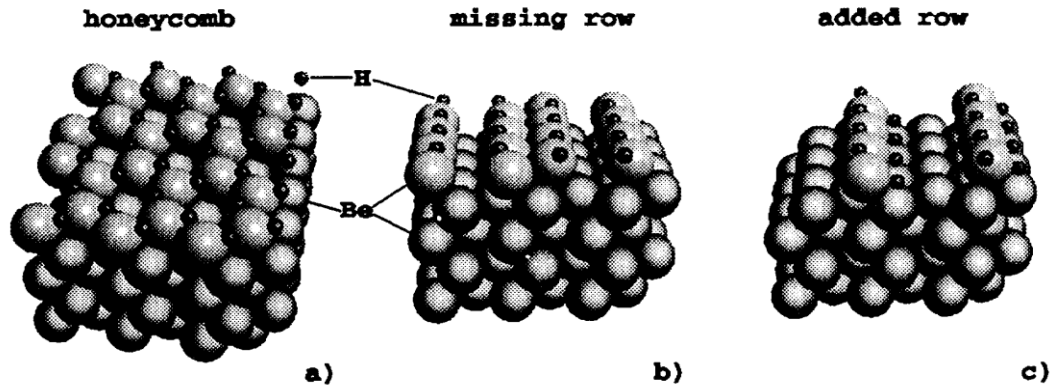


Figure 2: Possible H-induced surface reconstructions for Be(0001), taken from Stumpf & Feibelman (1994).

structural differences between the configurations of Figure 2, as well as disorder within them.

Given the importance of assessing the performance of beryllium in the tokamak environment, a number of the major confinement experiments (e.g. JET and ASDEX-Upgrade) have recently begun testing of new beryllium first wall components and coatings.¹⁵ As testing in these devices accelerates over the next several years, interest in hydrogen-beryllium interactions will certainly intensify. We view the work discussed here as a prerequisite for the development of reliable multi-scale computational models designed to predict the aggregate effects observed in linear plasma devices or tokamaks.

2.2 Low energy ion scattering and direct recoil spectroscopy

Figure 3 illustrates two collision geometries of interest for the work discussed here. The first configuration is used for low energy ion scattering (LEIS), whereas the second is typical for direct recoil spectroscopy (DRS). Both techniques use low energy (<5 keV) noble gas ion beams (typically He⁺ or Ne⁺) to probe the structure and composition of surfaces. The main difference between the two approaches is whether the scattered incident ions (as with LEIS) or recoils from the substrate/adsorbate (as with DRS) are analyzed. Both species contain useful information on the surface composition and structure.

While hydrogen is invisible to most surface techniques (including LEED, Auger electron spectroscopy, among others), it has been known for quite some time that LEIS and DRS are uniquely sensitive to light adsorbates. Pioneering work on this topic has been published previously by Bastasz¹⁶, Grizzi¹⁷, and others. The general procedure for detecting adsorbates involves angling incident ion beam at grazing incident with respect to the surface. Under these conditions, the energy of the incident ions perpendicular to the

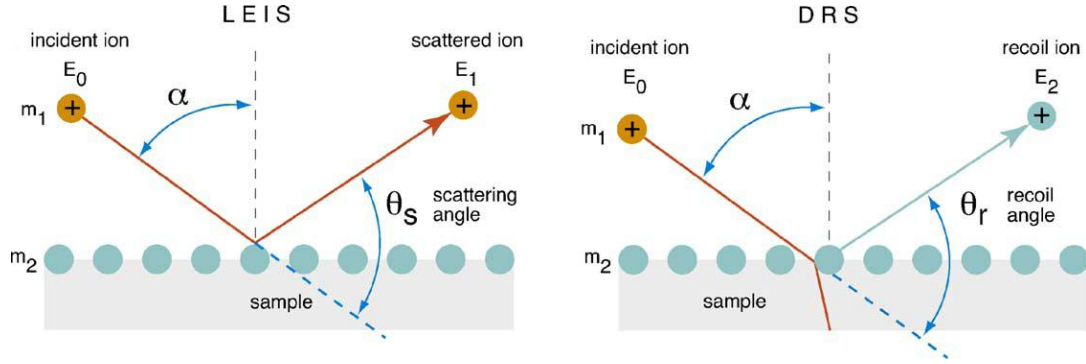


Figure 3: Scattering geometry for LEIS and DRS. [Image from R. Bastasz, et al., *Fusion Eng. & Design*, **72**, 111 (2004)] In both cases we consider an incident ion impinging on the surface at an angle α reference to normal, with initial energy E_0 and mass m_1 . The mass of the surface atom involved in the collision can be determined from: $\cos \theta_s = (1 + A)\sqrt{E_s} + (1 - A(1 - Q_n)) / \sqrt{E_s}$, where θ_s is the scattering angle, $A = m_2/m_1$ is the mass ratio, $E_s = E_1/E_0$, and $Q_n = Q/E_0$. A similar expression can be derived for the recoiled particles.

surface is very small, and the surface atoms gently steer the ions along open surface channels. If hydrogen atoms reside in these open surface channels, the incident ions will collide with them, thereby increasing the detected hydrogen recoil intensity.

One challenge associated with interpreting results from LEIS and DRS has been extracting detailed structural information from the measurements. The simplest way to model the surface collisions involves using analytic expressions to estimate how ions are deflected around surface atoms. (This is often referred to as a shadow cone; see Ref. 18 for further details.) While useful as a quick approximation, this procedure rarely provides anything more than a rough estimate of the surface structure. Nevertheless, for many years this type of rudimentary analysis was the main method of interpreting scattering measurements.¹⁹

A major advance in scattering models involved applying binary-collision codes to the problem. For computational efficiency, these codes (as their name suggests) use the binary collision approximation (BCA), where all collisions are considered discrete events involving only two partners. Although the BCA is rather restrictive, such codes do allow fairly complex sequences of distinct binary collisions to be simulated. In many cases, the calculated scattering intensities produced with this approach yield a fair approximation of experimental results. For many years, a barrier to carrying out such simulations was the need to accumulate adequate statistics for comparison with experiments. Most scattering calculations use a Monte Carlo approach, where one considers a large number of collisions over a representative area of the surface (usually a single unit cell.)

While a significant improvement over analytical techniques, BCA simulations are incapable of accurately reproducing the complex collision sequences that occur at grazing ion incidence. This is because the scattering process becomes more complex under these

conditions, with this incident ions interacting with many surface atoms at a given instant. This suggests that molecular dynamics simulations could be a useful alternative to simulating low energy scattering. The key hurdle associated with this approach has been that the simulations tend to be computationally intensive. However, if measures could be taken to improve the efficiency of such models, the current availability of highly automated instrumentation and increased computing power should make it practicable to undertake such an ambitious simulation project.

(This page intentionally left blank.)

3 Experimental hardware

We performed our hydrogen adsorption measurements using an angle-resolved ion energy spectrometer (ARIES.) This instrument was developed and refined at Sandia over many years and has been specifically modified for surface science studies geared toward detecting light adsorbates. A diagram showing the inner details of the ARIES source and analysis chamber is depicted in Figure 4. (Note that for clarity the electrostatic analyzer has been omitted.)

The instrument uses a mass separated, low energy (500 eV – 3 keV) ion beam (typically consisting of He⁺, Li⁺, or Ne⁺) to probe surfaces. The source itself is commercially available (Colutron), but was heavily modified with the addition of custom Einzel lenses, steering plates and apertures. The incident beam passes through a mechanical bend that separates neutral impurities. The resulting beam has an energy spread of ~1 eV at an incident energy of 3 keV (measured by passing the beam directly into our electrostatic analyzer.) One can vary the ion flux to the target over a range between 10¹³-10¹⁴ cm⁻²s⁻¹. The beam itself is rastered over a 2 mm × 2 mm area. The width of the raster is adjusted depending on the beam angle of incidence to ensure that spot size on the sample surface is maintained at a relatively constant size.

The beam passes into a turbo-pumped analysis chamber maintained at a base pressure of 8×10⁻¹⁰ torr. The chamber itself is equipped with a sophisticated sample manipulator that allows for translation along three axes, and rotation along two. The manipulator itself is stepper motor-controlled, enabling precise positioning of the sample with respect to the incident beam. The scattered ions are detected using an electrostatic analyzer mounted onto a rotatable platform. The entrance aperture to the analyzer is 2 mm in diameter, and is located 18.5 mm away from the sample. The entire system is computer-controlled, allowing for the execution of highly automated experimental test runs.

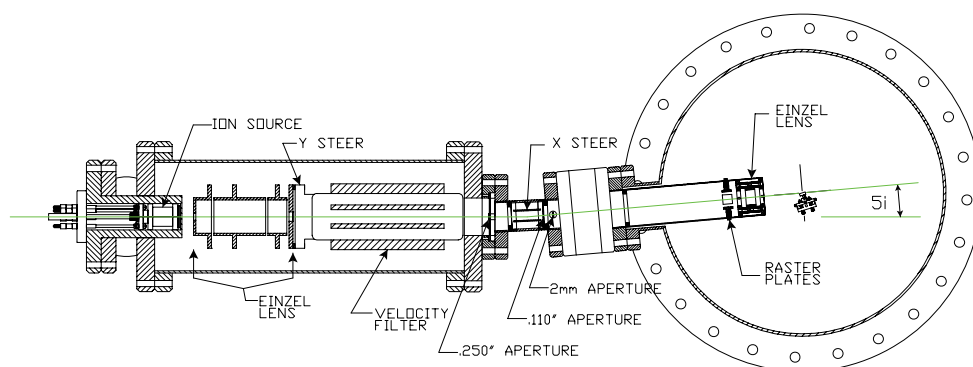


Figure 4: Schematic illustrating the interior details of the angle-resolved ion energy spectrometer (ARIES) at Sandia/CA.

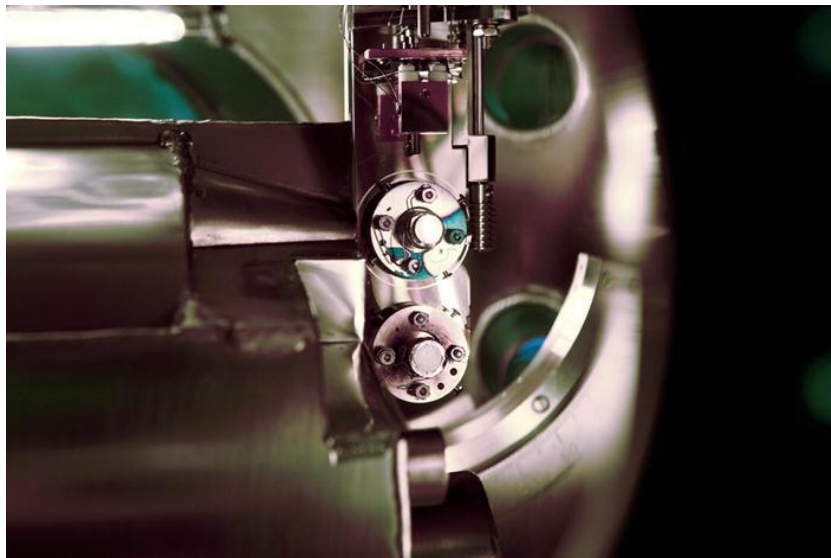


Figure 5: Image showing the ARIES sample manipulator. The electrostatic analyzer is visible in the foreground. (Only the top stage is rotatable.)

Figure 5 shows the end of the sample manipulator within the vacuum system. Two different samples can be accommodated at once, although only the top stage is rotatable. The samples can be exchanged without breaking vacuum using a magnetic manipulator arm (a particularly handy convenience for switching samples between different vacuum chambers.) To allow for different temperature regimes to be investigated, the beryllium samples used in this study were attached to a button heater with a sapphire disk sandwiched in between. This enabled temperatures up to 1000 °C to be maintained. For many surfaces (including beryllium), there is a large barrier to dissociative chemisorption of $\text{H}_2(\text{g})$. To aid in covering surfaces where this process is not favorable, our system is equipped with an atomic hydrogen doser consisting of a tungsten capillary that is heated by electron bombardment to 1800 °C, sufficient to create a beam of atomic H.

To aid in the experiments undertaken in this project, we also added an electron gun for Auger spectroscopy, as well as detectors for time of flight measurements. Because this hardware is described in later sections, we do not provide further details here.

4 Analyzing polycrystalline beryllium surfaces

One of the key technical challenges we needed to address with our work was the ability to demonstrate direct hydrogen on beryllium surfaces, in addition to ensuring that a clean surface can be readily maintained when dosing with atomic hydrogen. Our initial experiments enabled us to determine the optimal experimental configuration for detecting surface-adsorbed hydrogen. The LEIS measurements were performed using monoenergetic beams of low energy (0.5-3 keV) He⁺ and Ne⁺ ions. Figure 6 illustrates the experimental geometry; forward scattered and recoiled particles are collected by an electrostatic energy analyzer at discrete observation angles θ . Surface contaminants were removed by cycles of Ar⁺ sputter cleaning and annealing.

The energies of scattered and recoiled particles provide information about surface composition. An oxide forms on beryllium surfaces when exposed to H₂O or O₂, which can affect how hydrogen interacts with the material.²⁰ To provide the best sensitivity to chemisorbed O, we obtained 1 keV He⁺ scattering spectra from sputter-cleaned Be, as depicted in Figure 7(a). Note that the x-scale is normalized by the incident beam energy E_0 . The notation (s) and (r) indicates peaks associated with different scattering and recoil processes, respectively. The strongest signal arises from He⁺ scattering from Be, which is much more prominent relative to the oxygen peak. Considering the comparatively larger scattering cross-section for O under these conditions, this result indicates a relatively contamination free surface.

In an effort to improve our sensitivity to adsorbed hydrogen, we switched to 3 keV Ne⁺ ions which provide a larger recoil cross-section. Figure 7(b) shows ion energy spectra for both clean and dosed surfaces. During hydrogen dosing, a H(r) peak becomes quite prominent at a relative energy of $E/E_0=0.12$. Equally important is the absence of an O(s) peak in this spectrum which, if present, would appear at $E/E_0=0.8$. This verifies a dynamically clean surface can be maintained during H-dosing.

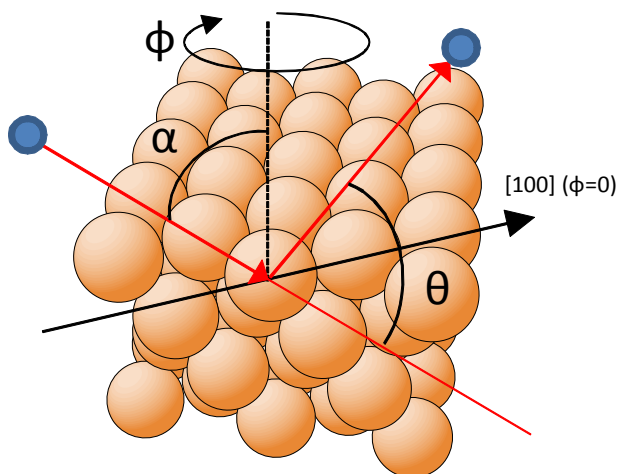


Figure 6: Scattering geometry for LEIS experiments, illustrating incidence (α), azimuthal (Φ), and observation (θ) angles.

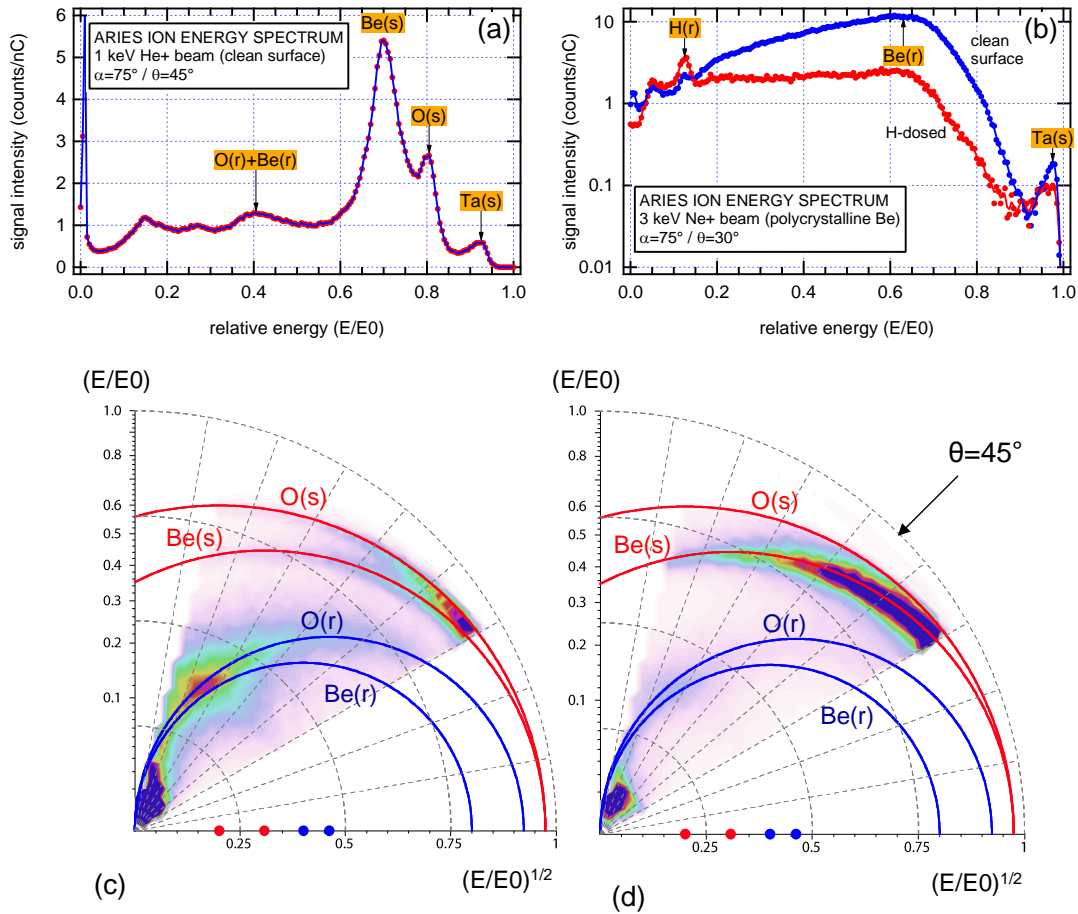


Figure 7: Ion scattering signals obtained from polycrystalline samples. Panel (a) depicts the scattering spectrum for 1 keV $\text{He}^+ \rightarrow \text{Be}(0001)$, (b) illustrates the $\text{H}(r)$ signal from a sample dosed with atomic hydrogen. Panels (c) and (d) show scattered ion signals for contaminated and clean surfaces, respectively. In both cases, the incident ions were 1 keV He^+ .

Peak locations in ion energy spectra depend on the scattering or recoil angles and, to a lesser extent, inelastic energy losses. One can select the observation angle θ to optimize the balance between signal strength and peak separation. Figs. 1(c) and 1(d) illustrate the variation of ion signals with θ for 1 keV $\text{He}^+ \rightarrow \text{Be}$ at an incidence angle of $\alpha = 15^\circ$. (Note that darker coloration reflects a higher scattering yield.) These polar plots use a normalized energy for the radial coordinate $\sqrt{(E/E_0)}$, whereas the angular coordinate is θ . When rendered in such a manner, the locations of scattering and recoil peaks map onto circles and can be calculated analytically assuming inelastic losses are small, as indicated by the red and blue circles. Note that the ion energy spectrum in Figure 7(a) corresponds to a radial cut in Figure 7(d) (represented by the line at $\theta = 45^\circ$.) Such polar plots can provide a clear way to differentiate between different elements present on the surface.²¹ This is illustrated by the differences between Figs. 1(c) and (d), which correspond to oxygen contaminated and clean Be surfaces, respectively. The $\text{O}(s)$ signal is much more

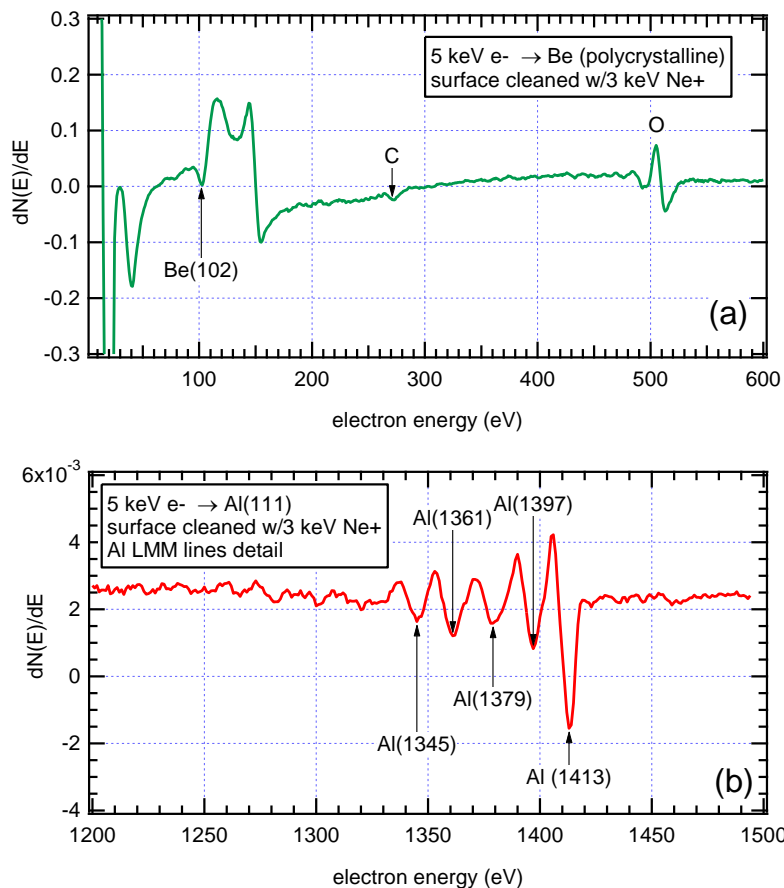


Figure 8: Auger electron spectroscopy results for Be and Al surfaces, shown in panels (a) and (b), respectively.

intense in the oxide contaminated case and is easily distinguished from the Be(s) signal at large θ . Similarly, for 3 keV $\text{Ne}^+ \rightarrow \text{Be}$ (not shown) small scattering angles ($\theta \approx 30^\circ$) reveal the best separation between the hydrogen recoil peak and other signals.

4.1 Characterizing adsorbed oxygen with Auger electron spectroscopy

Beryllium quickly forms an oxide layer when exposed to small amounts of impurities. While LEIS and DRS enable identification of surface-adsorbed species, the Ne^+ ion beam probes do not provide a strong scattering signal from lighter elements such as C and O. To supplement these measurements, we added an electron gun to our system to enable Auger electron spectroscopy (AES) measurements. AES is highly sensitivity to both surface impurities. By monitoring the amplitudes of the O and C *KLL* transition peaks in the derivative AES spectrum, we verified that surface contaminants were reduced to negligible levels during the preparation of the surface. One benefit of our system was that we were able to use the same electrostatic analyzer for the Auger analysis by simply reversing the bias on the hemispheres.

For this purpose we added a Kimball Physics electron flood gun capable of reaching energies of up to 5 keV. Samples were prepared using a 3 keV Ne⁺ ion beam. Our hemispherical analyzer was positioned to collect electrons emitted normal from the surface, whereas the electron beam was at an incidence angle of 60°. The spectra were collected simultaneously with the ion bombardment.

In Figure 8(a), we show an AES derivative spectrum for a Be surface. In this case, a small amount of contamination is visible on the surface, and as a result the KLL transition peaks associated with O and C are readily visible. When the surface was completely clean these peaks could not be distinguished from the background. At energies <200 eV, some erratic structure is visible. This structure was always present in our Auger spectra, although its exact structure changed depending on ion bombardment and analyzer settings.

The Auger spectrum for beryllium is not particularly remarkable, since there is only one peak associated with it (located at 102 eV.) With this in mind, we have also included a Auger spectrum for a clean Al(111) crystal, as shown in Figure 8(b). This spectrum was acquired for the polycrystalline case. The Al Auger spectrum is a bit more interesting since the LMM lines are also visible. We verified that these lines occur at the expected locations for Al.

5 Analyzing single crystal beryllium surfaces

5.1 Sample preparation

Beryllium single crystals are not commonly available, likely due to hazards associated with polishing. For our experimental work, we used a crystal from the inventory within the Radiation-Solid Interactions Department at Sandia/NM. The crystal itself originated from the Franklin Institute in Philadelphia. The sample itself measured 5 mm × 4 mm × 3 mm, and had been cut so that the largest surface was roughly aligned with (0001) plane.

One of the few laboratories capable of polishing and aligning single crystal materials is the Surface Preparatory Laboratory in Amsterdam, The Netherlands. A Laue diffraction pattern confirmed the orientation of the crystal, and allowed for alignment to within 0.5° of the Be(0001) surface plane. The Laue pattern is shown in Figure 9. Note that the Laue spots show some sign of mosaic structure. For many surface techniques, this would be a serious problem. However, ion scattering is fairly robust against small imperfections in the crystal. Such imperfections would superpose a uniform “background” to our measurements, without significantly altering the structural observations.

As an example of the type of structural information that can be revealed with this approach, consider Figure 10, which shows an experimental scattering map our group recently obtained for a clean, unreconstructed Be(0001) surface using a 1 keV He⁺ ion beam probe. The map coloration indicates the scattering intensity, whereas the spatial coordinates correspond to distance from a “reference” lattice site at the center of a map. In this case, we have used the formalism developed by Agostino et al.²² as an expedient way to render the maps in real space. This allows us to superimpose the actual positions of the first-layer beryllium atoms (indicated by the blue circles). The intensity patterns within the map are largely due to how the incident ions are blocked or “shadowed” by neighboring atoms, making them directly sensitive to surface atom positions. A rough prediction (based on Oen’s empirical fit¹⁸) of the shadowing due to each surface atom is indicated by the dashed curves. The experimental scattered ion signals are strongest in between these lines, where the incident ions are focused along open surface directions.

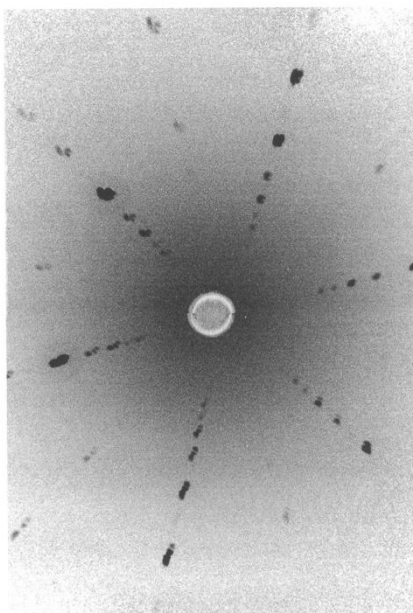


Figure 9: Laue pattern for the Be(0001) sample used in this study.

The scattering map can be used to verify the configuration of the surface (in this case the clean Be(0001) surface is verified to be non-reconstructed.) It also enables us to verify the orientation of the Be crystal. However, perhaps most importantly, the scattering maps provide a comprehensive overview of scattering processes on the surface, illustrating how ions are focused along open surface channels in the absence of adsorbed hydrogen. The presence of adatoms on the surface will disrupt these processes, as will be discussed in the next section.

5.2 Hydrogen-dosed experiments

We were able to detect distinct H(r) signals from the sample when dosed with low levels of atomic H. To perform the H dosing measurements, we feed research-grade H₂ through an atomic doser heated to 1700 °C by electron bombardment. We varied the partial pressure of H within the chamber between 10⁻⁹ – 10⁻⁶ torr to achieve different levels of surface coverage. A competing effect is the removal of surface hydrogen by the incident ion beam. However, a partial pressure of 10⁻⁸ torr or larger was sufficient to ensure that the arrival rate of H to the surface overwhelmed the removal rate by the incident beam.

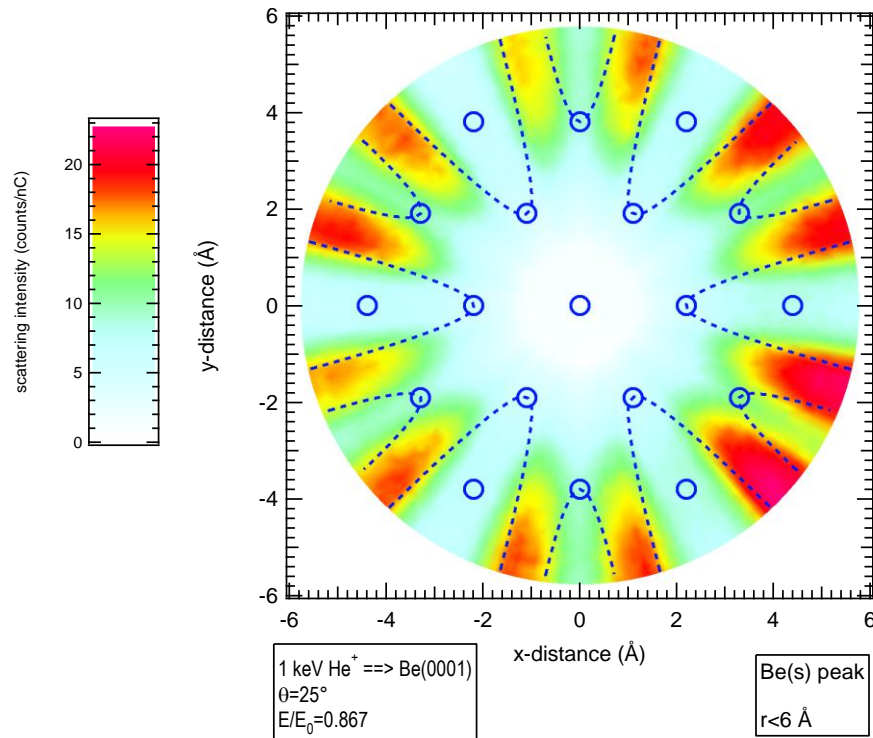


Figure 10: Real-space scattering map of the Be(0001) surface, measured recently during experiments at Sandia. The map coloration indicates scattering intensity, whereas the positions of first-layer Be atoms (and shadowed areas) are indicated in the overlay.

Determining the amount of H₂ that could be bled into the chamber without contaminating the surface required considerable care. We found that at dose levels >10⁻⁷ torr, the surface remained clean initially, but then slowly became contaminated with time. The main culprit appeared to be residual H₂O that arose during dosing. By operating the doser at a low temperature (to prevent outgassing of the surrounding equipment), and reducing the H₂ flow rate, we were able to mitigate this problem.

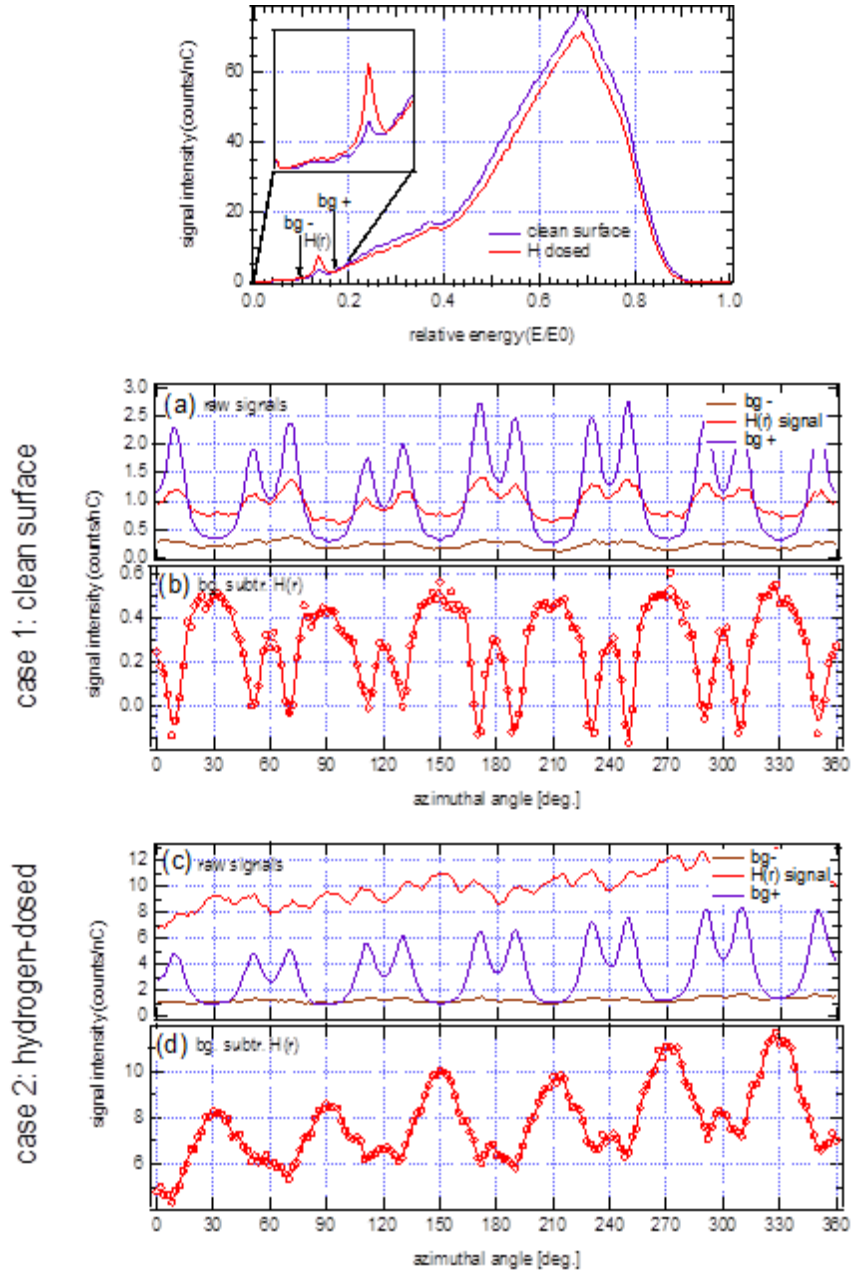


Figure 11: Recoil signals from low-coverage hydrogen exposures of Be(0001).

With the aforementioned problems resolved, we were able to proceed resolving the hydrogen behavior on the surface. First, consider the spectra shown in Figure 11, which shows the presence of H(r) and Be(r) signals. Note that the H(r) peak resides on the tail of the much larger Be(r) peak. Small variations in the stronger signal could easily overwhelm any structural information that could be obtained from the smaller one. Therefore, to determine how this signal varies with azimuth (especially at low dose rates), background subtraction was required. Points on either side of the H(r) peak were monitored (labeled

here “bg+” and “bg-”); the background level was determined by linear interpolation. To minimize statistical noise in the subtraction process, we increased the ion beam dwell at each azimuth.

Using this process, we were able to observe the hydrogen recoil variation with azimuth. The recoil intensity reached a peak every 30°. A comparison with the scattering map illustrated in Figure 11 reveals the peak in recoil intensity occurs along the <100> directions. This indicates that hydrogen resides within open surface channels on the surface. Extracting more detailed information requires a more sophisticated modeling approach. The next chapter describes the development of the modeling framework needed to address this challenge.

(This page intentionally left blank.)

6 Developing a new theoretical framework for modeling scattering experiments

Note: As part of the research program, we developed a modeling framework for simulation low energy ion scattering measurements. This work has been accepted for publication:

R. D. Kolasinski, N. C. Bartlet, J. A. Whaley, and T. E. Felter, *Phys. Rev. B* **85**, 115422 (2012).

(This page intentionally left blank.)

7 Time of flight system for impact collision ion scattering spectroscopy (ICISS)

A key accomplishment of this program has been the development of a time-of-flight (TOF) spectroscopy system for our ARIES instrument. To determine ion energies, our electrostatic analyzer (ESA) biases two hemispheres relative to each other. Only ions within a narrow energy range are able to travel between the hemispheres and into a Channeltron electron multiplier. Such systems have commonly been used for surface science applications, and have the advantage of being relatively straightforward to operate. They also offer superior energy resolution (our system can distinguish peaks separated a fraction of an eV.) However, an ESA only detects charged particles. Since most of the particles scattering from surfaces are likely neutrals rather than ions, much information is missed by this type of detector.

An alternative to the more conventional ESA setups is TOF spectroscopy. As the name implies, the ion flight times are used to calculate ion energies. To use this approach, one must make the assumption that a “packet” of incident ions arrive at the sample at a single point in time. These ions undergo collisions with various surface species, and in the process lose different amounts of energy. This results in a distribution of flight times to a TOF detector. To create an ion packet in a practical experimental setting, one typically sweeps the incident ion beam across an aperture. This of course results in an ion packet of finite width. This is not a significant concern so long as the packet width (~ 10 ns) is much smaller than the flight times (~ 10 μ s).

In this study, we have added two TOF detectors to our system. The first of these is positioned at the exit of the ion source, enabling us to detect directly back-scattered particles. The second detector was added behind the entrance aperture to the ESA. The following sections describe the details and testing of these detectors.

7.1 Detecting backscattered particles: Impact collision ion scattering spectroscopy

In this study, we added an annular micro-channel plate detector and the accompanying electronics to our ARIES system. This instrumentation enables us to perform impact collision ion scattering spectroscopy (ICISS), where ions which have been directly backscattered are detected. ICISS is a specialized variant of ion scattering spectroscopy where the scattering angle is nearly 180° . Since the directly backscattered particles are unlikely to undergo complex multiple collision events, analyzing the scattering data is simplified greatly. Furthermore, the new system enables neutral particles to be measured as well as ions, eliminating the need to account for neutralization in our modeling. (Our present electrostatic analyzer is capable of measuring only charged particles.) Since ions typically comprise only a small fraction of the scattered particles, the TOF instrumentation reduces the dose required to obtain scattering spectra considerably. The TOF detector is positioned at the exit of the ion source. It consists of a stack of two 40 mm diameter micro-

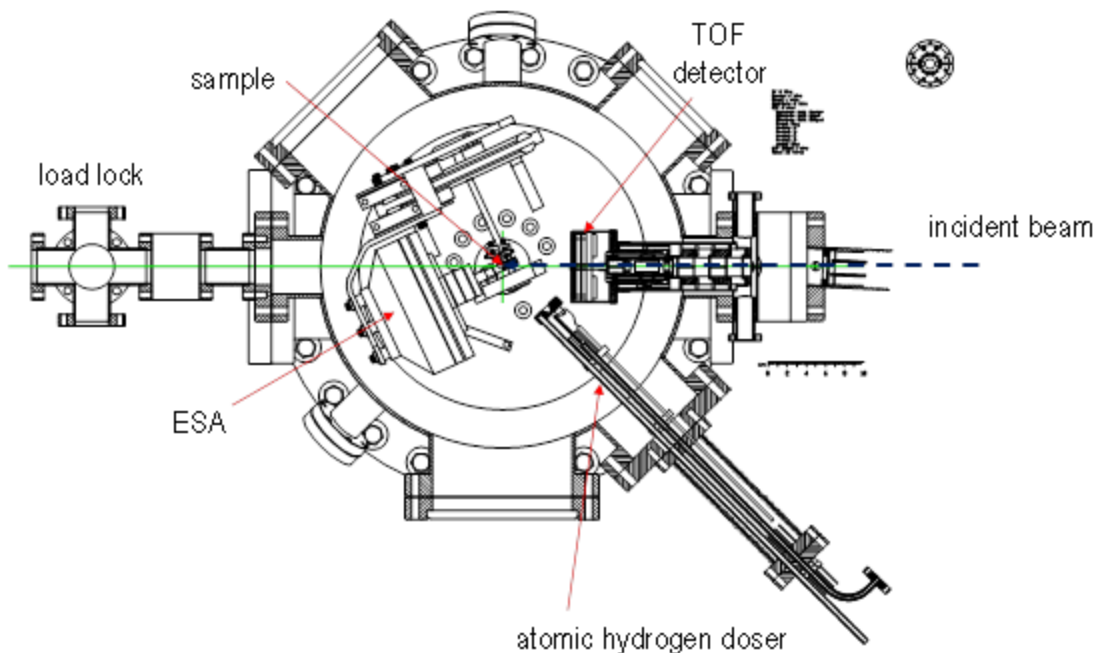


Figure 12: Schematic of ARIES analysis chamber showing TOF and ESA detectors.

channel plates (MCPs) with a small hole cut in the center. The hole enables the incident ion beam produced by the ARIES source to pass through it. This allows us to match the 180° scattering angle needed to collect the directly backscattered particles as closely as possible.

A diagram of the TOF detector is shown in Figure 12, and the electronics needed to collect the spectra are shown in Figure 13. The timing for the entire system is controlled by a delay generator, which can output a variety of pulse shapes at precisely timed intervals. At the start of the timing sequence, the delay generator commands a HV pulser to apply a high voltage to the x-steering plates in the ARIES beam line. (About 340 ns is required for the pulser to respond to this initial command.) Once the voltage pulse is applied, the beam is swept across an aperture downstream. This effectively creates a well-defined “ion packet” needed for the TOF measurements. The HV pulse width is adjustable between about 40 ns to 1000 ns. The width of the beam pulse is defined by the rise time of the high voltage pulser, which in this case was 7 ns. As the pulser turns off, the beam is swept across the aperture once again, resulting in the production of a second ion packet. A longer delay time would be desirable so as to eliminate this second sweep, but for the initial tests described here the spacing between the two pulses was large enough that there was no interference.

After the ion packet is created, it travels down the ARIES beam line to the sample over a length of 14.65 in. Backscattered ions are then collected by the detector, which is positioned 3.125 in. behind the sample. The detector accepts ions which are scattered between $\theta=165^\circ-178^\circ$. In future iterations of this work, we will work to correlate the timing data with the scattering angle, but this angular range is narrow enough to provide

reasonable energy resolution. To prevent stray electrons from reaching the detector, we bias a high transmission grid in front of the detector to a modest voltage, typically -100 V.

The flight times are measured using a time to amplitude converter (TAC). At the same time the delay generator initiates the HV sweep on the x-steering plates, it also sends a "START" pulse to the TAC to begin acquisition. The TAC then measures the amount of time elapsed until a "STOP" pulse is received. Ideally, this "STOP" pulse should coincide as closely as possible with the instant an ion strikes the front micro-channel plate. To minimize any delays associated with processing electronics, we measure the pulse from the ion impact directly from the back side of the second micro-channel plate. A fast-preamp amplifies the signal, and a constant fraction discriminator produces a fast NIM pulse which is used to provide a "STOP" signal to the TAC. The delay introduced by these processing steps is in the pico-second range, much smaller than the flight times expected for these experiments. Taking into account the dead times of the detector and electronics, the above process can be repeated up to a rate of about 30 kHz.

To validate the new detection system, we examined flight times from different materials. Figure 14(a) depicts flight times for 3 keV He⁺ atoms scattering from an Al surface. We have corrected for a small offset in the TAC at its lower range, so the spectrum is slightly offset from t=0. As previously discussed the HV pulse is produced 340 ns after the TAC is started. (A small amount of noise is picked up by our electronics immediately after this pulse.) The 3 keV He⁺ ions have a velocity of about 3.8×10^5 m/s, and require 978 ns to traverse the 14.65 in. distance from the x-steering plates to the sample. For Al the backscattered ions then require 284 ns to traverse the 3.125 in. distance back to the detector. The expected arrival time of the backscattered He at the detector is indicated in the figure; the associated peak is located just behind this. The delay is likely due to inelastic losses. (Also the distance between the sample and detector is adjustable via the positioning stage, and therefore also needs to be calibrated.)

While this approach worked effectively for surfaces such as Al and stainless steel, we had difficulty applying it to beryllium. The reason for this is the mass of the beryllium surface atoms was not much larger than the incident He⁺ atoms. As a result, they backscattered with energies of only ~200 eV, where the sensitivity of our detector begins to decline. Adsorbed impurities such as O tended to overwhelm the Be signal, making it difficult to extract detailed structural information.

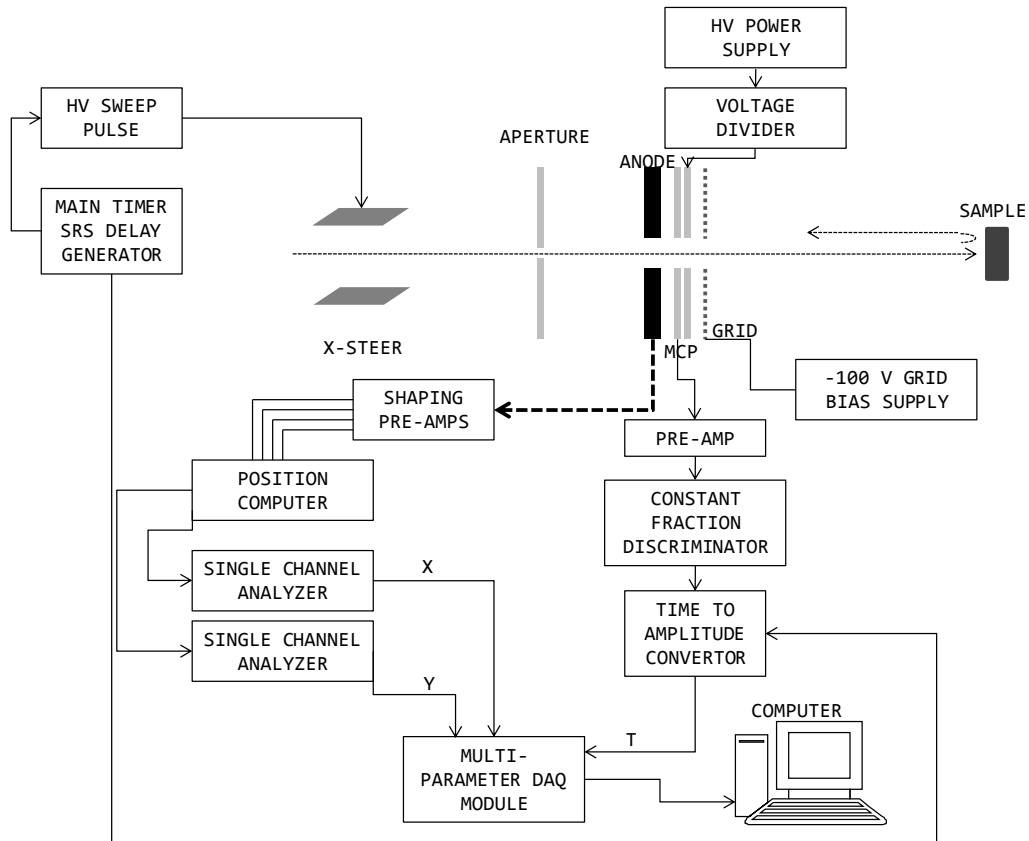


Figure 13: Schematic of time-of-flight system electronics.

Note that the spectra in Figure 14 were acquired over 1000 s using an average beam current of 0.05 nA – corresponding to about 4 orders of magnitude less current than was previously required to acquire a reasonable signal using the ARIES electrostatic analyzer (~500 nA)!

In Figure 14(a), we show three different spectra, each for different pulse widths for the sweep voltage applied to the x-steering plates. As previously discussed, the pulse length that could be achieved was limited to 1000 ns. As a result, a second ion packet is produced as the HV pulser turns off. The backscattered ions from this second ion packet are also recorded by the TAC equipment and are responsible for the second peak in each of the TOF spectra. Here we consider 3 different pulse widths: 40 ns, 300 ns, and 500 ns. The second peak is delayed by an amount corresponding to the pulse width.

Finally, in Figure 14(b), we compare the 3 keV He⁺→Al TOF spectra to one obtained for 3 keV Ne⁺→stainless steel. (Note that the noise floor for each system is a bit different.) The different flight times for each ion-target combination correspond reasonably well with the predicted values, thereby helping to validate our approach. With an improved system for pulsing, it should be possible to greatly improve our energy resolution.

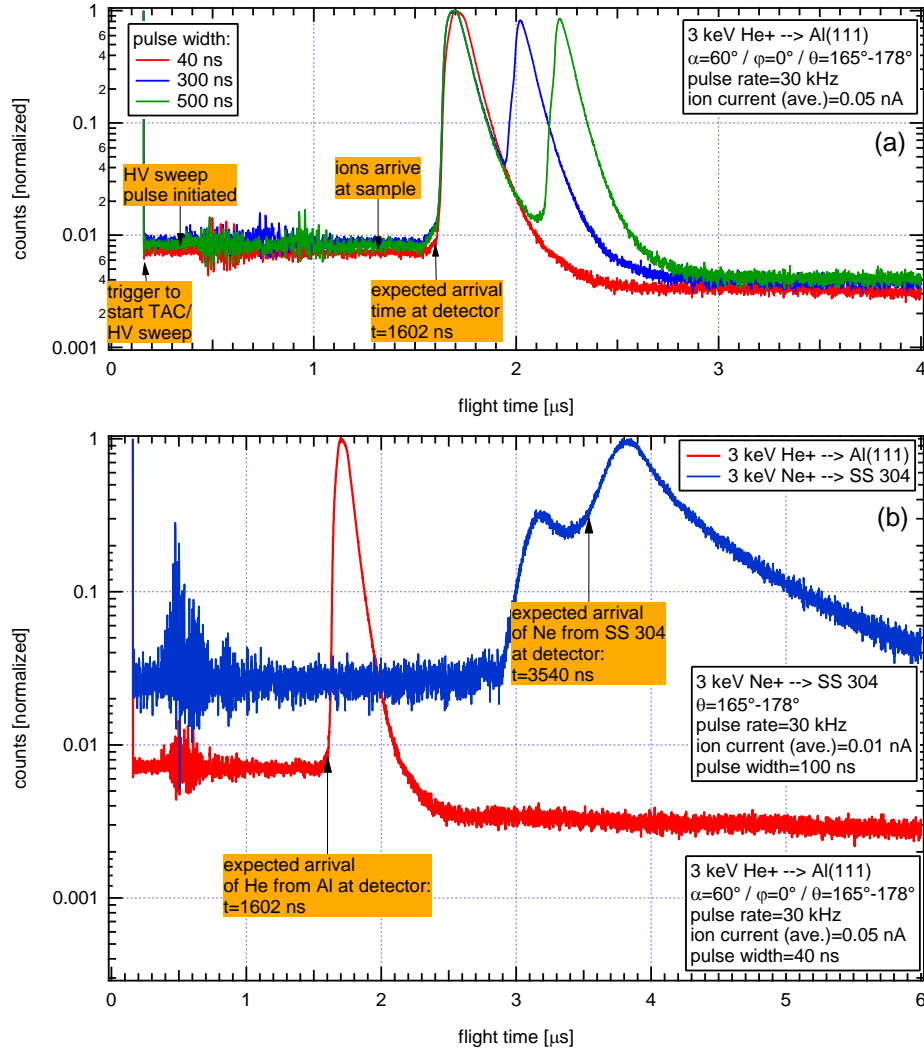


Figure 14: Time of flight spectra showing the effect of (a) varying the pulse width and (b) changing the materials examined.

7.2 Detecting forward scattered particles via time-of-flight

We also added a second micro-channel plate detector to allow us to detect forward-scattered particles. Previously, we obtained this type of information from our electrostatic analyzer. Modeling neutralization of low energy ions is complex, so the ability to detect both neutrals and ions enables us to simplify our modeling approach significantly. The micro-channel plate detector was attached to the exit of our hemispherical analyzer. When the hemispheres of the ESA are biased, ions will be separated out of the flux to the detector. We have successfully installed this new detector in our system, but are still in the process of fully testing it.

(This page intentionally left blank.)

8 Summary of Results / Outlook

The Be(0001)+H system has been sparsely studied, and the results presented in this report represent one of the few characterizations of this fundamental system. Using DRS, we were able to observe the behavior of hydrogen on this surface. Undoubtedly, this information will be especially valuable in developing fundamental models of hydrogen on surfaces, as well as basic models of recycling from surfaces relevant to magnetic fusion.

The time of flight system developed here will also enable a wealth of new experiments. By reducing the dose required to obtain a measurement by 10^4 , the technique becomes essentially non-destructive, enabling us to characterize delicate surfaces or thin films with precision. The ability to distinguish ions from neutrals in a quantitative manner will allow us to probe the electronic properties of surfaces.

Finally, the modeling framework developed here makes it possible to rigorously model scattering from surfaces at grazing incidence. We describe further pathways forward along these directions in the following section.

8.1 Future modeling pathway

Our previous work shows that MD, when coupled with accurate physical inputs, reproduces the experimentally-observed hydrogen recoil signals satisfactorily.²³ However, the gap between this accomplishment and the next step in developing the computational framework needed to simulate routinely ion scattering is much larger than simply moving these simulations to a cluster with many processors. The results depicted in the previous section included many simplifying assumptions specific to the W(100)+H(ads) system, some of which may not apply to more general systems.

We were somewhat fortunate in our previous work that the W(100)+H(ads) surface, at saturation coverage, is not reconstructed and includes relatively simple open surface channels that were easy to model. With this in mind, it was possible to consider a simplified substrate that included only atoms along these surface channels. Under these constraints, a usable surface model therefore could be as small as 100 atoms. A disadvantage to this approach is that it limits us to considering conditions where the incident ions were aligned to within $\pm 15^\circ$ of the channel. (Larger misalignments would cause the incident ions to escape to another part of the surface.) Even with these simplifications, each test case depicted in Fig. 5 required ~ 1 week to execute on a single processor. For the more complex structures possible with Be (such as the three reconstructions depicted in Figure 2), the geometry is not nearly as favorable. This is particularly true for the surface vacancy structure in Figure 2(a). Furthermore, step edges and other surface imperfections are present in the experimental system, and their effect must be accounted for in our models. At this level of complexity (when the simulation domain is likely to include thousands of atoms), advanced parallel computing becomes a necessity.

The pathway for accomplishing this clearly calls for using a more sophisticated surface model. The basic MD package we have been using (Kalypso²⁴) was designed with sputtering simulations in mind and is intended for serial execution. For this reason, it is certainly not suitable for solving large-scale MD problems. A viable alternative is LAMMPS, a public domain MD code developed at Sandia and designed specifically for use on large-scale parallel machines. For a detailed discussion of the algorithms contained therein, we direct the reader to Ref. 25.

A key advantage of LAMMPS is its flexibility – it can be readily customized to allow us to refine the physics inputs to our MD model. An important step in this process, as previously discussed, involves incorporating improved scattering potentials to account for the ion-target interactions of interest. Only the short-range repulsive portion of the potential is needed for the colliding species, and in our prior approach we neglected any interaction between substrate and adsorbate atoms during the scattering process. This assumption, while reasonable in most circumstances, may be violated under circumstances where the interaction between the substrate atoms becomes important. Accounting for these effects will require including more accurate long-range potentials for Be-H and Be-Be interactions. Additional effects treated only in a rudimentary way in our preliminary studies include thermal vibrations and neutralization. One would expect that these would have a much more modest effect on the scattering simulations, however uncertainties introduced by these inputs need to be well understood.

References

- ¹ G. Federici, et al., Nucl. Fusion **41**, 1967 (2001).
- ² B. D. Wirth, K. Nordlund, D. G. Whyte, and D. Xu, MRS Bull. **36**, 216 (2011).
- ³ K. B. Ray, J. B. Hannon, and E. W. Plummer, Chem. Phys. Lett. **171**, 469 (1990).
- ⁴ K. Pohl and E. W. Plummer, Phys. Rev. B **59**, R5324 (1999).
- ⁵ K. L. Wilson, J. Nucl. Mater. **103 & 104**, 453 (1981).
- ⁶ P. Andrew, et al., Nucl. Fusion **33**, 1389 (1993).
- ⁷ J. Hogan, P. Mioduszewski, L. Owen, T. Uckan, and C. Klepper, J. Nucl. Mater. **196-198**, 1083 (1992).
- ⁸ C. Grisolia, L. D. Horton, and J. K. Ehrenberg, J. Nucl. Mater. **220-222**, 516 (1995).
- ⁹ R. A. Causey and K. L. Wilson, J. Nucl. Mater. **212-215**, 1436 (1994).
- ¹⁰ R. A. Causey, J. Nucl. Mater. **300**, 91 (2002).
- ¹¹ T. Vegge, Phys. Rev. B **70**, 035412 (2004).
- ¹² D. F. Johnson and E. A. Carter, J. Mater. Res. **25**, 315 (2009).
- ¹³ R. Stumpf and P. J. Feibelman, Phys. Rev. B **51**, 13748 (1995).
- ¹⁴ K. Christmann, R. J. Behm, G. Ertl, M. A. V. Hove, and W. H. Weinberg, J. Chem. Phys. **70**, 4168 (1979).
- ¹⁵ G. F. Matthews, Phys. Scr. (in press).
- ¹⁶ R. Bastasz, T. E. Felter, and W. P. Ellis, Phys. Rev. Lett. **63**, 558 (1989).
- ¹⁷ O. Grizzi, M. Shi, H. Bu, J. W. Rabalais, R. R. Rye, and P. Nordlander, Phys. Rev. Lett. **63**, 1408 (1989).
- ¹⁸ O. S. Oen, Surf. Sci. **131**, L407 (1983).
- ¹⁹ H. Niehus, W. Heiland, and E. Taglauer, Surf. Sci. Rep. **17**, 213.
- ²⁰ R. Bastasz, (Sandia National Laboratories, 1984).
- ²¹ R. Bastasz, J. W. Medlin, J. A. Whaley, R. Beikler, and E. Taglauer, Surf. Sci. **571**, 31 (2004).
- ²² R. G. Agostino, P. Aebi, J. Osterwalder, J. Hayoz, and L. Schlapbach, Surf. Sci. **384**, 36 (1997).
- ²³ R. D. Kolasinski, N. C. Bartelt, J. A. Whaley, and T. E. Felter, Phys. Rev. B (submitted).
- ²⁴ M. A. Karolewski, Nucl. Instrum. Meth. B **230**, 402 (2005).
- ²⁵ S. Plimpton, J. Comput. Phys. **117**, 1 (1995).

(This page intentionally left blank.)

Distribution:

1	MS 0899	RIM -Reports Management	9532 (electronic copy)
1	MS 0359	Donna L. Chavez, LDRD Office	1911



Sandia National Laboratories